Radiation Enhancement by Nonequilibrium in Earth's Atmosphere

Chul Park*
NASA Ames Research Center, Moffett Field, California

The status of knowledge of shock-layer radiation in the low-density nonequilibrium regime, as appropriate to the flight of the proposed aeroassisted orbital transfer vehicle, is surveyed. The existing laboratory data and the flight data from Apollo and Fire are scrutinized. Nonequilibrium radiation is found to be significant in the flight regime of the vehicle, but a factor-of-three uncertainty is found in its magnitude. The available theoretical models are reviewed, their weaknesses are pointed out, a computer code that approximately reproduces the existing data is introduced, and recommendations are made for future research.

Nomenclature

A = reference surface area of a vehicle
A_{ij} = rate coefficient of radiative transition from state i to state j
B_{ij} = matrix consisting of collisional and radiative transition rates in the left-hand side of quasi-steady-state master equation (9)
C_d = drag coefficient
c_i = vector in the right-hand side of quasi-steady-state master equation (9)
D = diffusion coefficient
G = gravitational constant
g = statistical weight of an internal state
h = altitude
h_i = enthalpy of species i
I = intensity of radiation
I_s = specific impulse of a rocket engine
K_{ij} = rate coefficient of collisional transition from state i to state j
k = thermal conductivity
Le = Lewis number
M = mass of vehicle
N_e = electron number density
n = number density of an internal state
n_i = number density of state i
Pr = Prandtl number
p = pressure
q = heat flux
R_f = forward reaction rate
R_r = reverse reaction rate
T = heavy-particle translational temperature
T_e = electron translational temperature
t = time
u = flow velocity in tangential direction
V_∞ = flight velocity
X = number density of unspecified species
x = distance from shock wave
α = species mass fraction
ϵ = ionization fraction
ρ = density

Subscripts

c = convective
cw = convective component at wall
e = equilibrium
ne = nonequilibrium
r = radiative
rw = radiative component at wall
0.1 = the point where radiation is 10% higher than it is at equilibrium

Presented as Paper 83-0410 at the AIAA 21st Aerospace Sciences Meeting, Reno, Nev., Jan. 10-13, 1983; received March 7, 1983; revision received June 19, 1984. This paper is declared a work of the U.S. Goverment and therefore is in the public domain.

*Reseach Scientist, Computational Chemistry and Aerothermodynamics Branch. Member AIAA.

Introduction

WITH the advent of the Space Shuttle, the frontier in space has moved one step outward. A bulk of the future space activity is expected to take place in the near-Earth orbits. In the field of transportation systems, the activity could involve commuting between various space satellites or stations. The vehicle proposed for such missions is referred to as an orbital transfer vehicle (OTV).[1,2] The performance of the OTVs can be improved, at least theoretically, if they are allowed to fly through Earth's atmosphere and if they can decelerate or maneuver using aerodynamic forces.[3] This idea leads to the so-called aeroassisted orbital transfer vehicle (AOTV).

Because of its intrinsic requirements and constraints, an AOTV must fly in the high-altitude, low-density region at a near-escape velocity. In such an environment, the shock layer around the vehicle is likely to produce significant radiation and a heat shield must be provided to protect the vehicle from it. Therefore, in order to carry out a conceptual design of such a vehicle, one must be able to calculate the radiative heat fluxes to the vehicle.

During the Apollo era, the problem of radiation was studied extensively through laboratory and flight tests. It was found in the laboratory studies that radiation is enhanced significantly in the low-density regime because of the lack of chemical equilibrium. The extent of radiation emission found in these studies is such that it would be a serious problem in AOTV operation. In contrast, tests conducted aboard the Apollo vehicles (and the Fire vehicles that were associated with the Apollo program) have shown little radiative heat transfer in the low-density regime; that is, they show no such radiation enhancement. The cause of this discrepancy between laboratory and flight data has not yet been determined and, without knowing the cause, it is difficult to predict the effect of nonequilibrium radiation on AOTV. On the other hand, the techniques of predicting radiative heat-transfer rates for chemically equilibrium flows have been improved greatly in recent years, primarily because of Project Galileo.

The purpose of the present paper is to survey the status of the knowledge of radiation in the nonequilibrium regime that is appropriate to the flight of AOTVs. In the first part, the problem is examined from the programmatic and empirical points of view. To do so, the reasons why AOTVs must fly in the low-density regimes are first delineated. The essential findings of the laboratory studies of nonequilibrium radiation for the low-density regime are then reviewed and the Apollo and Fire flight data are analyzed to determine the cause of the absence of radiation enhancement in those flights. In the second part, the nonequilibrium radiation problem is reviewed from a theoretical viewpoint. The gas kinetic phenomena (chemical reactions and diffusion) affecting the gas properties in the low-density regime are first examined. Next, the radiation mechanisms in the nonequilibrium region that are different from the equilibrium cases are summarized; the limits of present-day knowledge of the physical quantities involved and the ability to numerically compute the phenomena are surveyed; and an approximate computing method that drastically simplifies the physical picture (but still yields results that are within a factor of three of the laboratory data) is presented. Finally, suggestions are made about the directions that future research in radiation enhancement should take.

Empirical Considerations

Missions for Aeroassisted Orbital Transfer Vehicles

Many artificial satellites are in orbit around Earth. Most commercial communications satellites occupy the geosynchronous orbit (GEO), which is at an altitude of about 36,000 km and is on the plane passing through the equator. The orbit most easily accessed from the continental United States, that is, the one that requires a minimum amount of fuel to ascend to, is at an altitude of (typically) 400 km and is on the planes that intersect the equatorial plane at an angle of about 30 deg. These low Earth orbits (LEO) are to be used by the Space Shuttle as a staging or parking orbit. The corresponding LEOs used by the Soviet Union are at orbital angles of about 60 deg.

If, as envisioned, space manufacturing and space medicine become realities in the future, these LEOs will be permanently settled by humans. Various Earth-surveying and space-studying satellites occupy orbits in the altitudes varying between those of LEO and GEO with orbital angles varying from 0 deg (equatorial) to 90 deg (polar). A proposal has been made also that the lunar libration centers be colonized.[4] The libration points L1-L5 are unique in that not only do they offer valuable scientific opportunities, but a minimum amount of rocket fuel is required to descend from them to intersect any given orbit around Earth. If space vehicles could be decelerated by means of aerobraking, virtually no fuel would have to be expended in rendezvousing with any targeted satellite in the LEO. For this reason, such vehicles would be best suited for emergency rescue or policing operations.

It would be of great value if one could travel between one satellite station and another. A vehicle that could do so is presently referred to as an orbital transfer vehicle (OTV).[1,2] With an OTV one could tow a decommissioned unmanned satellite for repair and refurbishing and resupply manned or unmanned satellites. The OTVs must perform two basic types of operations: altitude change and orbital plane change (Fig. 1). The most notable examples of altitude change would be transporting commercial communications satellites to and from the GEO and commuting to and from the libration centers. Orbital plane changes would be required most frequently to make transfers from one to another satellite in the LEO.

To carry out an altitude-change maneuver without the use of aerobraking, two rocket engine burns must be executed, one at the higher and the other at the lower orbit. For the GEO-to-LEO transfer, the velocity changes required are about 1.5 and 2.4 km/s at the high and the low orbits, respectively. The amount of fuel required to achieve a specified velocity change ΔV is given by the well-known rocket equation

$$M_i/M_f = \exp[\Delta V/(GI_s)]$$

where M_i is the initial mass (= final mass + fuel mass), M_f the final mass, G the gravitational constant, and I_s the specific impulse. With a rocket engine with specific impulse of 280 s attainable with storable fuels, the two engine burns would require initial-to-final mass ratios of about 1.7 and 2.4, respectively. The L5-to-LEO transfer would require a near-zero velocity change at the libration point and a 3.8 km/s change at the LEO, corresponding to a mass ratio of about 4. The transfer from a Space Shuttle orbit to a polar orbit would require a velocity change of about 6 km/s and a mass ratio of 9.

Aerobraking and aeromaneuvering will reduce the fuel requirements greatly. For the altitude changes, the engine burns at the lower altitude are unnecessary. Saving in fuel will result in orbital plane change also if the vehicle has a lift-to-drag (L/D) ratio greater than 1, since such a vehicle will

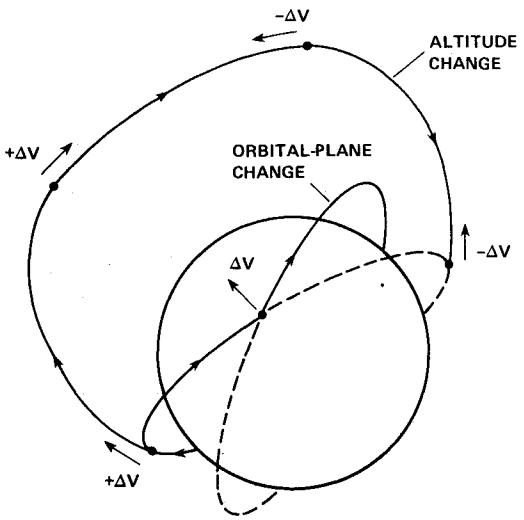

Fig. 1 Two main OTV missions.

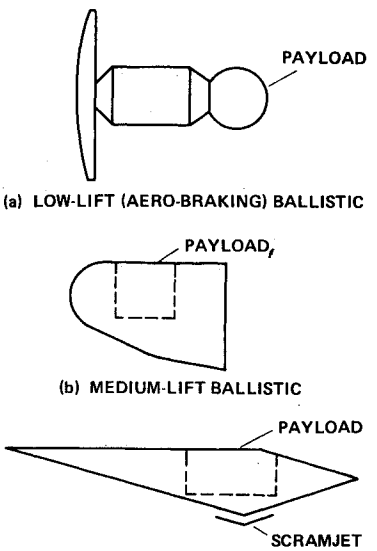

Fig. 2 Three generic types of AOTVs.

acquire a greater normal velocity change than the velocity loss due to drag.[3] Ideally, an orbital-plane change could be accomplished by an aeromaneuvering vehicle of high L/D equipped with an airbreathing engine.[5] In most practical cases, an altitude change will accompany a minor orbital-plane change. A blunt-nosed ballistic vehicle with a medium built-in lift will be useful for this purpose. Such reasoning leads to the three generic types of vehicles (all AOTVs) shown schematically in Fig. 2.

The heat shielding requirements for these different types of AOTVs are nearly the same, provided their size and the ballistic coefficients are the same. These two main parameters can be estimated from the following considerations:

1) Mass: The commercial satellites of the future are expected to have a mass of about 5000 kg or more. To tow such a payload, the total mass at the time of atmospheric entry will be about 10,000 kg or more.

2) Size: The overall diameter of typical commercial satellites is of the order of 5 m. The fuel tank and crew's compartment will have a similar size. To protect these components from the entry heating, the overall diameter of the heat shield must be about 10 m. In Fig. 3a, a conceptual AOTV is shown schematically and is compared with the Apollo vehicle and the spacecraft called Fire that were flown to simulate the Apollo entry flights. As shown here, the proposed AOTVs are larger and have a smaller ballistic coefficient.

Figure 4 shows typical flight trajectories of the AOTV with a ballistic coefficient given in Fig. 3a (84.9 kg/m^2) and compares them with those of the Apollo and Fire vehicles. As seen in these figures, the entry velocities of the AOTVs are nearly identical to those of the Apollo or Fire vehicles. But the AOTVs are in the high-altitude range (about 70 km) longer than either the Apollo or Fire vehicle. Because of the relatively large size of the vehicles and the low ambient density at high altitudes, the convective heat-transfer rates to the vehicles are relatively small, that is, less than 100 W/cm^2. By means of injection, the convective heat-transfer rate can also be reduced.[1] However the large body size produces a thicker shock layer and, consequently, greater radiative heat-transfer rates to the body. One must therefore examine the effects of the radiative heating rates on the AOTVs.

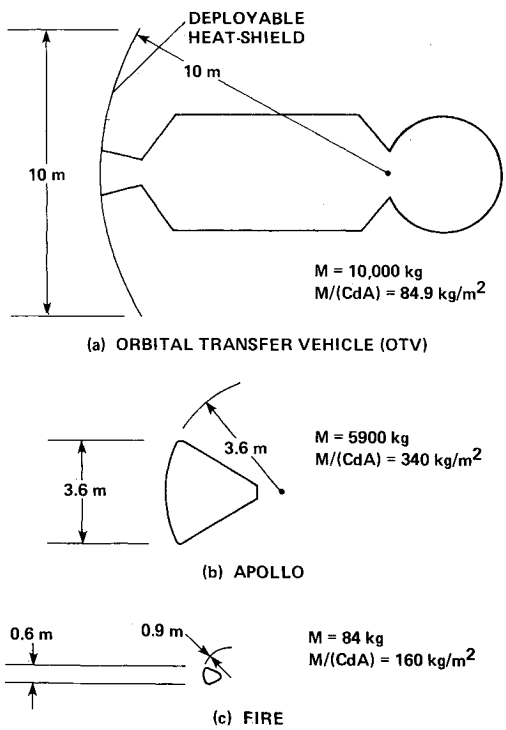

Fig. 3 Typical dimensions of AOTV, Apollo, and Fire vehicles.

Laboratory Data

Before the flights of the Apollo, a concerted effort was made to determine the radiative heat-transfer rates to the vehicles. Shock-tube and ballistic range experiments were conducted and theoretical calculations were made. Shock tubes were operated[6-8] at shock velocities up to 10 km/s. There was a lower limit on the gas density in these tests because of the intrinsic limitations of a shock tube, such as boundary-layer growth and contact-surface broadening. At the shock velocity of 7 km/s, the lowest tested charging pressure ahead of the shock wave was 0.05 Torr, which corresponds to an altitude of about 70 km (see Fig. 4a). At the shock speed of 10 km/s, the lowest tested pressure was 0.1 Torr, corresponding to an altitude of 65 km. The tested velocity-density regimes are compared with those of the AOTVs in Fig. 4a. In order to overcome the difficulty caused by the boundary-layer growth, the tests were conducted with large shock tubes (diameters of 15 cm). The radiation emanating from the hot gas was measured with a sensor located outside the tube from the so-called "side-on" position, as shown in Fig. 5a.

The shock-tube experiments showed that the luminosity of air is zero immediately behind a shock wave, rises to a peak, and decays to a small value, as shown schematically in Fig. 6. This radiation overshoot phenomenon was interpreted as being due to chemical nonequilibrium and a qualitative explanation was easily given. A nitrogen molecule has a relatively large binding energy (9.8 eV) and hence requires a long time to dissociate. Before it could dissociate to its equilibrium level, the temperature rose to a higher level than the equilibrium value, which in turn is believed to cause the observed luminosity overshoot.

The luminosity of the gas at its peak intensity I_p, the luminosity in the equilibrium region I_e, the time to reach the peak intensity t_p, and the time for the luminosity to reach 1.1

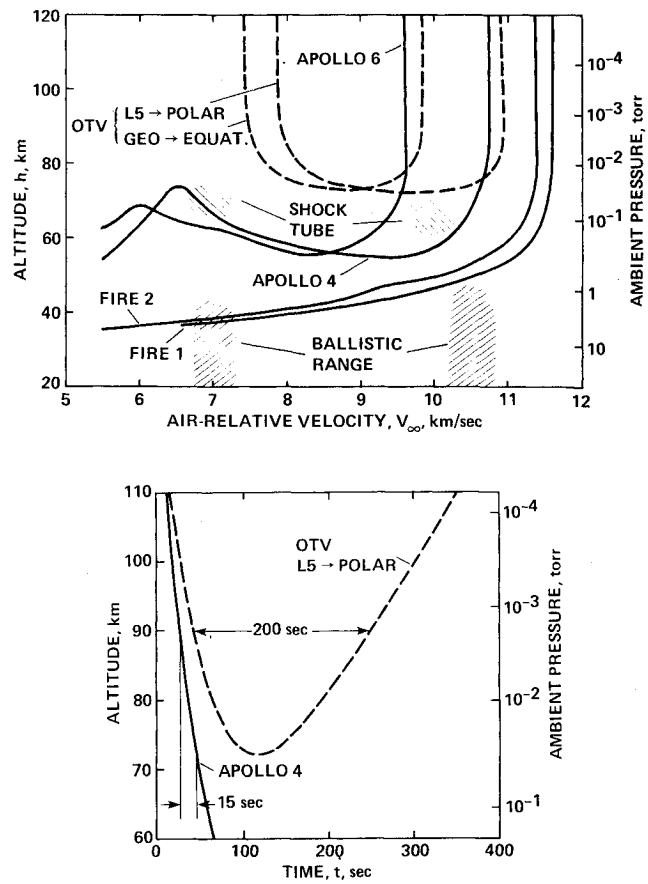

Fig. 4 Flight trajectories of AOTV, Apollo, and Fire.

times I_e $t_{0.1}$ (see Fig. 6) have been measured over a wide range of gas densities and shock velocities. It was found that, at least in the visible and infrared wavelength ranges, I_p varies approximately proportionally with the gas density and t_p and $t_{0.1}$ vary approximately inversely with the gas density. The area under the luminosity curve integrated up to $t_{0.1}$ remained approximately constant over a range of gas densities for a fixed shock velocity. This property is called a "binary scaling" law of nonequilibrium radiation.[6-8] Assuming that the gas radiation is optically thin, the radiative power emission per unit volume was obtained by dividing the observed radiative power into the side-on direction by the path length of the emitting medium.

The radiative heat flux in the direction of gas flow, that is, in the end-on direction shown in Fig. 5c, was then calculated by multiplying the power emission per unit volume by the thickness of the gas in the end-on direction. This heat flux from the nonequilibrium region of the shock layer q_{ne} obtained in the shock-tube experiments is shown in Fig. 7. The equilibrium region that follows the nonequilibrium region also emits a small amount of radiation. From any given shock layer, therefore, the radiation reaching the wall of a vehicle is the sum of the nonequilibrium radiation q_{ne} and the radiation from the equilibrium region q_e. If the residence time within the shock layer is smaller than $t_{0.1}$, equilibrium radiation is absent and the nonequilibrium radiation does not reach its full extent. This premature termination of nonequilibrium radiation owing to lack of flow residence time was name the "truncation" effect.[6-8]

Similarly, in the ballistic range experiments, the total radiation emitted by a shock layer and received by a sensor located at a side-on position is determined (see Fig. 5b).[9,10] This measured radiation is presumed to be a sum of that from the nonequilibrium region and that from the equilibrium region, integrated over the entire visible portion of the shock layer. Over a finite range of flow conditions, the measured radiation intensity was found to be nearly independent of gas density. This phenomenon was interpreted as being caused by the binary scaling of nonequilibrium radiation. In this range, therefore, radiation is presumed to be from the nonequilibrium region only. The nonequilibrium radiation data obtained by this method are shown in Fig. 7, where they are compared with shock-tube data. The two sets of data agree to within a factor of about four. Shown also in the figure is the result of a calculation made using an approximate theory that will be described later in this paper.

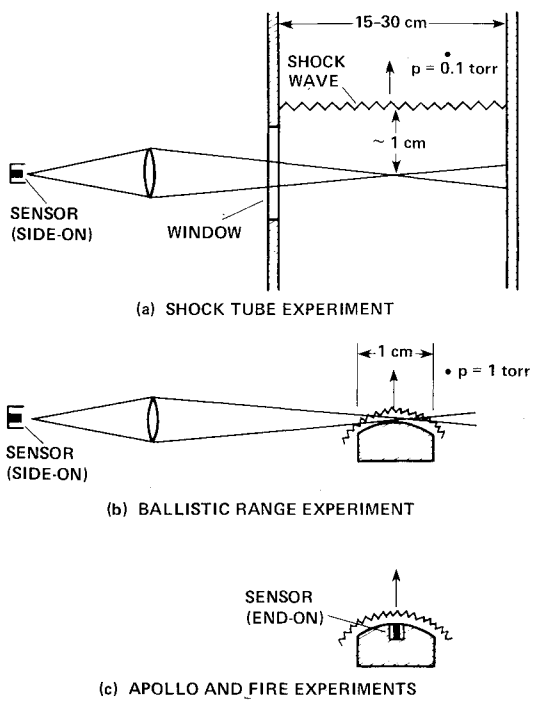

Fig. 5 Schematic of experimental methods for determining radiative heat-transfer rates.

Apollo Experience

Subsequent to these laboratory studies, the Fire 1 and 2 vehicles, equipped with convective and radiative heat flux gages at various points, including the stagnation point, were launched into the atmosphere (Fig. 5c).[11,12] The Fire vehicles were approximately ¼-scale models of the Apollo command module vehicle and entered the atmosphere at velocities slightly in excess of those of Apollo vehicles (see Fig. 4). The Fire vehicles were made of beryllium and hence were not ablating. The measured convective heat-transfer rates agreed well with the predictions made using the available theories. The radiation data at the low altitudes also agreed well with the equilibrium radiation predictions,[11,12] but the measured radiative heat fluxes in the high-altitude range were considerably smaller than those deduced from the laboratory data (see Fig. 8). Instead of being invariant with respect to density, as was predicted by the binary scaling law, the measured radiative heat flux diminished with diminishing flow density. An examination of the flight environments revealed that such deficiency occurred in the regime of densities lower than those tested in the shock tubes. This prompted the investigators to speculate that the binary scaling law is violated a very low densities because of a lack of sufficient molecular collisions to maintain the excited-state populations.[11,12] Based on the premise that the excitation of atoms and molecules occurs through the collisions among those atoms and molecules, such speculation seemed to be plausible: at the densities where the breakdown of the binary scaling law occurred, the rates of molecular collisions were of the same order as those of radiative depopulation of the excited states. The deficiency in the excited-state populations hypothetically caused by this phenomenon was called the "collision-limiting" phenomenon.[12] An empirical correction factor accounting for this collision limiting is derived from the Fire experiment, as shown by the chain curve in Fig. 8; it was used in predicting the radiative heat-transfer rates to Apollo vehicles.[12]

Before the manned flights, Apollo 4 and Apollo 6 were flown unmanned, equipped with calorimeters and radiometers, as were the Fire models.[13] The calorimeters were designed to measure the sum of the convective and radiative heat-transfer rates and the radiometers measured only the radiative components. These sensors were installed inside cavities made on the heat shield. The Apollo heat shields were made of phenolic-epoxy Novalak with glass reinforcements, which are known to pyrolyze and char at fairly low heating rates.[13,14]

Figure 9 shows the results of the calorimeter and radiometer measurements.[13] In the region where the nonequilibrium radiation is expected to dominate, that is, at altitudes above about 65 km, the measured radiative and convective heat-transfer rates were much smaller than those predicted with the binary scaling law and were similar to the radiative heat-

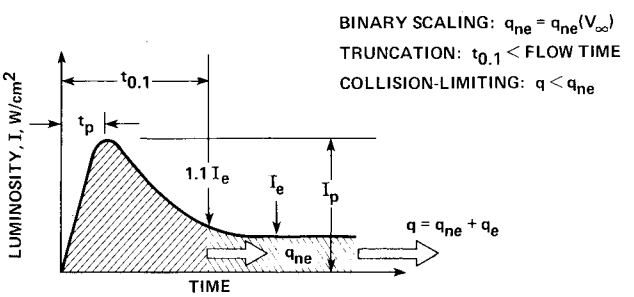

Fig. 6 Concepts of nonequilibrium radiation.

transfer rates observed for Fire models. Therefore, the Apollo tests seemed to validate the collision-limiting concept.

To understand the nature of the so-called collision-limiting phenomenon, the shock-layer flows in the stagnation region of the Fire and Apollo vehicles are analyzed in the present study for altitudes between 70 and 80 km at which the phenomenon was seen. In Fig. 10a, the enthalpy profile calculated for Fire 1 at the midpoint of its radiation measurement (altitude of 78.1 km), using the classical stagnation point boundary-layer theory, is shown by the solid curve. The profile is obtained assuming a fixed Prandtl number of 0.72 and corresponds to the case in which air remained in chemical equilibrium. In the ionizing regime, the Prandtl number is known to vary approximately as[15]

$$Pr=\frac{2}{3}\frac{1}{1+230\epsilon} \tag{1}$$

where ϵ is the ionization fraction. In the entry flight of Fire 1, the equilibrium flow calculation predicts an ϵ value of about 0.25 at the stagnation point, corresponding to a Prandtl number of about 0.01. Such a low Prandtl number occurs only at the very edge of the boundary layer for an equilibrium flow; as the temperature falls toward the wall, the Prandtl number rapidly increases toward 0.72. Hence, the boundary-layer profile can be determined approximately by assuming Pr to be 0.72. As shown in Fig. 10a, the edge of the equilibrium boundary layer extends almost to the shock wave in this case.

At the density regime of the flight of Fire 1, however, it is likely that the boundary-layer flow was chemically frozen. Hence, the electrons present at the edge of the boundary layer must have diffused toward the wall through the boundary layer. Assuming that the wall was fully catalytic to electron recombination,[16] the concentration of electrons in the boundary layer would vary smoothly from the edge value to the zero value at the wall, following the well-known diffusion profile of the stagnation point boundary layers. The Prandtl number would consequently remain small throughout most of the boundary layer. For this case, the stagnation point boundary layer is solved assuming a variable Prandtl number such that it agrees with the value predicted by Eq. (1) at the edge and varies as a simple power of enthalpy. The resulting enthalpy profile is shown in Fig. 10a (dashed curve). As seen here, the frozen boundary layer is predicted to extend farther than the position of the shock wave. Since this is impossible, one concludes that there was no discernible inviscid shock layer outside the boundary layer in this altitude range and that the shock layer was fully viscous. The nonequilibrium radiation was truncated severely as a result. The observed

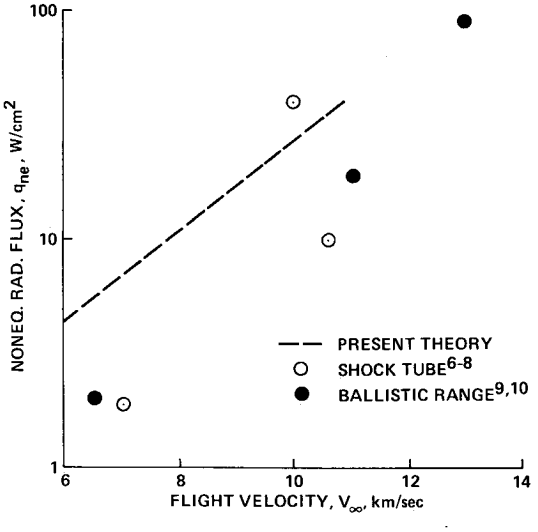

Fig. 7 Nonequilibrium radiative heat flux obtained in the laboratory.

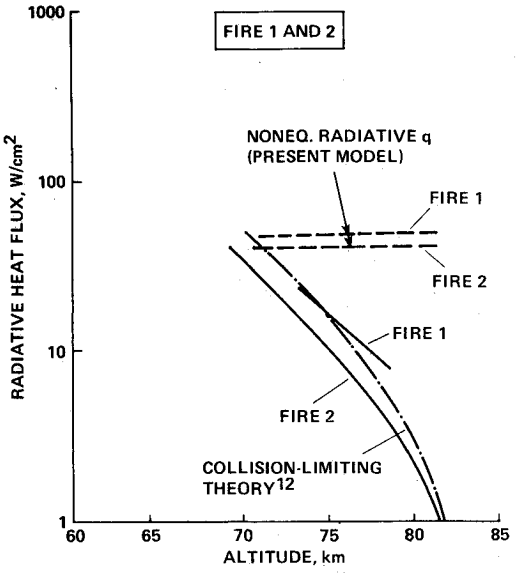

Fig. 8 Radiative heat flux for the Fire 1 and 2 vehicles.

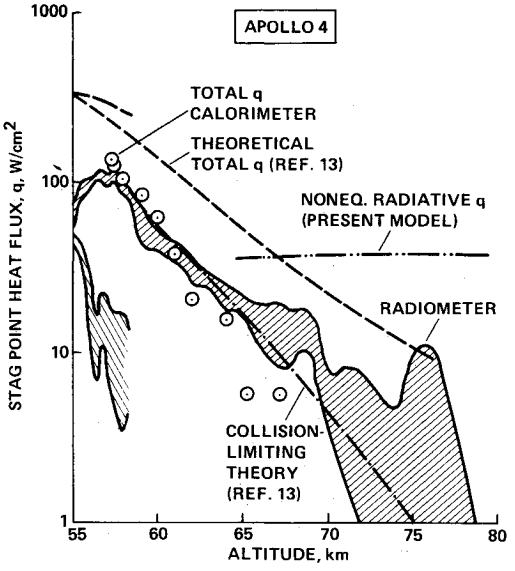

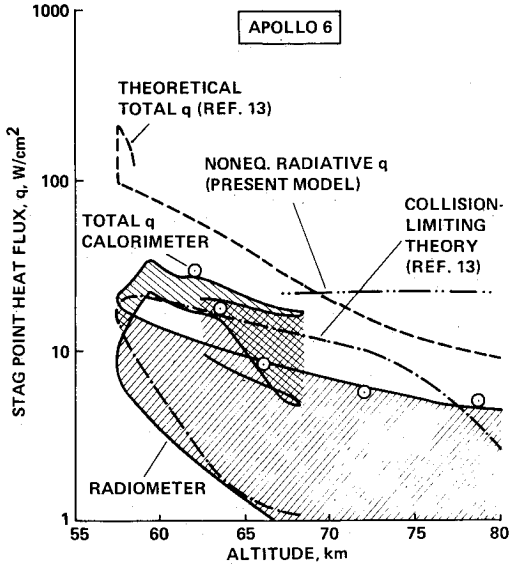

Fig. 9 Stagnation point heat-transfer rate data for the Apollo vehicles (Ref. 13).

deficiency in radiation can be explained by this truncation, even though this argument does not rule out a true, collision-limiting phenomenon.

In the case of Apollo, one notices first that the calorimeter and radiometer measured approximately the same heat fluxes in the high-altitude range. This can be true only if the convective heat-transfer rate is zero. In turn, it can be true if the boundary layer is blown severely by the gas injected from the wall, possibly by the ablation products of the heat shield material. To understand the phenomenon, an ablation calculation was performed in the present study, using an existing computer code designated CMA (charring material ablation).[17] The charring process of the Apollo heat shield cannot be modeled accurately because of the complexity of the chemistry of the material.[17] Hence, the pyrolysis phenomenon was first assumed to occur as for nylon-phenolic, for which the characteristics are better known.[18] For this calculation, the convective heat-transfer rate for the unblocked wall is determined by the formula of Fay and Riddell.[19] For the radiative heat-transfer rate, the observed radiative heat flux values are faired with a smooth curve (Fig. 11). The calculation yields a total mass loss of about 0.32 g/cm^2 at the stagnation point. The experimental data on Apollo[14] showed a mass loss of about 0.6 g/cm^2. Hence, the rate of mass loss calculated by this method, which assumed nylon-phenolic properties, is doubled in order to approximate the ablation phenomena for the Apollo heat shield. The chain curve in Fig. 11 shows the resulting wall convective heat-transfer rates. As seen here, the calculated all convective heat-transfer rates are fairly small. This explains, at least qualitatively, why the calorimeters and radiometers measured approximately the same heat fluxes.

Using the ablation rates so obtained, the boundary-layer flows are solved for Apollo 4 in the same manner as for Fire 1. In Fig. 10b, the enthalpy profiles so obtained are shown for all altitude of 73.5 km. As seen in Fig. 10b, the blowing layer occupies a major portion of the total shock-layer thickness, both for the equilibrium and nonequilibrium cases. As was true for Fire 1 (Fig. 10a), the frozen-flow boundary layer extends beyond the shock wave. One concludes, therefore, that the nonequilibrium radiation must have also been severely truncated at the high altitudes for the Apollo flights. One also notes here that such a thick ablation layer could have absorbed the radiation before it reached the wall. The blowing layer absorption can explain the hysteresis phenomenon observed for Apollo 6: as Fig. 10b indicates, the radiative heat flux at the altitude of 65 km is lower in the early part of the entry flight than in the later part, probably because the pyrolysis gas emission was stronger during the early period.

For both the Fire and Apollo flights, therefore, the true extent of nonequilibrium radiation was never measured. The collision-limiting concept cannot be substantiated at all, even though one cannot rule it out.

The theoretical argument leading to the collision-limiting concept, that is, that the excitation of atoms and molecules (by heavy particle collisions) is insufficient in the altitude ranges of 70-80 km, is also suspect. In the flight regimes of the Fire and Apollo vehicles, it is likely that the shock-layer flow was partly ionized. Electrons collide with atoms and molecules at rates two orders of magnitude faster than the collision rates of heavy particles. Moreover, electrons are very efficient in causing electronic and vibrational excitations: the existing data on the excitation of atoms by electrons indicate that the excitation cross sections for the optically allowed transitions are in fact larger than the elastic collision cross sections.[20] This reasoning leads one to believe that the collisional excitation rates were about two orders of magnitude faster than the radiative depopulation rates at the 80 km altitude.

Theoretical Considerations

Reliability of Laboratory Data

Since AOTVs will be larger than either the Apollo or Fire vehicles, the truncation phenomenon seen in Fig. 10 is less likely to occur. According to Fig. 7, the nonequilibrium radiative heat flux q_{ne} is between 10 and 100 W/cm^2, which is of the same order of magnitude as the convective heat-transfer rate for the AOTV. The equilibrium radiation will increase the wall radiative heat flux still further. Since the flights of the Fire and Apollo vehicles did not yield useful information on the magnitude of these radiations, one is compelled to rely on the laboratory data shown in Fig. 7 in the design of AOTV heat shields. It would seem prudent, therefore, to examine the reliability of the laboratory data.

In both shock-tube and ballistic range experiments, the radiation measurements were made side-on as shown in Fig. 5. In the case of the shock-tube experiment, the diameter of the tube was about 15 cm. Over such a path length, the assumption of optical thickness becomes suspect. At the center of an atomic or molecular spectral line, self-absorption is likely to occur even at the low-density regime of concern. By assuming the radiation to be optically thin, gas luminosity is underestimated. The optical depth of nonequilibrium radiation in the end-on direction toward the wall in a shock

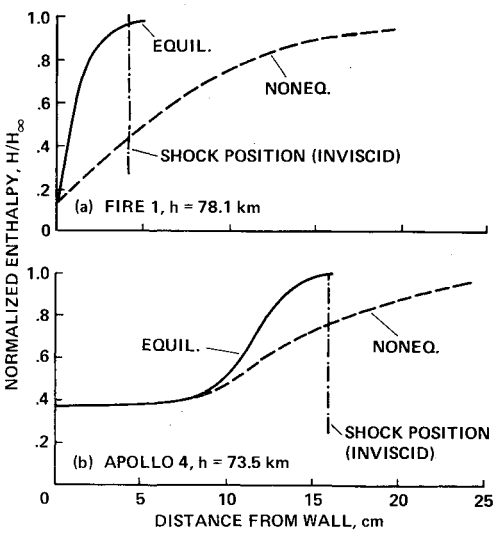

Fig. 10 Enthalpy profiles for the Fire and Apollo vehicles calculated assuming equilibrium and nonequilibrium chemistry.

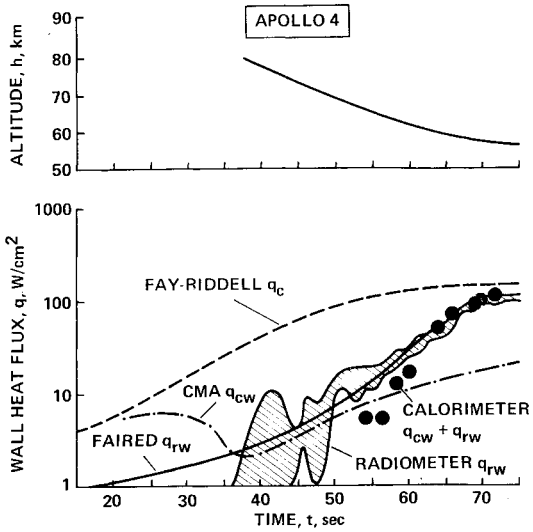

Fig. 11 Heat-transfer rate history for Apollo 4, combining measured data with CMA calculation.

layer is smaller than 15 cm (typically about 1 cm) and, hence, the optical thinness approximation holds closer. The procedure adopted results, therefore, in an underestimation of the true radiative heat flux into the blunt body. This underestimation of radiation is more pronounced at the low shock velocities where ionization is absent—because the spectral lines are narrower in such regimes and hence more self-absorption occurs.

The same argument holds for the ballistic range data. Although the physical sizes of the models were small in the ballistic range tests, the densities of the freestream gases were relatively high to avoid the truncation phenomenon. The total optical depth in the side-on direction is considerably larger than into the end-on direction, as is apparent from Fig. 5b. One suspects, therefore, that both shock-tube and ballistic range test data are likely to underestimate the true radiative heat fluxes to the vehicle.

In addition, for the ballistic range experiments, a complicated volume integration of the emitting medium had to be carried out in order to determine the radiative power emission per unit volume, which involved an assumption about the distribution of gas properties throughout the shock layer, and the accuracy of the assumption is not fully understood. Ideally, a radiation measurement can be made from an end-on position, as was done for the Apollo and Fire vehicles. This will eliminate the uncertainty about the optical thickness and the emitting volume. Both the shock tube and ballistic range could be used for such an end-on measurement, with complementing advantages and disadvantages.

Chemical and Kinetic Relaxation

In view of the uncertainties in the experimental radiation data in the low-density regime, it would seem worthwhile to attempt an alternative, theoretical approach. In the following two sections, the status of the knowledge of the subject is reviewed.

A prerequisite to computing radiation is knowledge of species concentration and controlling temperatures. In general, there are four different modes in sensible temperature, that is, gas (heavy particle), rotational, vibrational, and electron. These quantities are governed by the equations of conservations of species mass, global mass, global momentum, global energy, energy in individual sensible mode, and momentum of electron gas (electric current). The general forms of these equations are well known.[16,21] In the low-density regime being considered, the transport phenomenon enters into all of these equations.

The rate of change of mass fraction of a chemical species α is a sum of the rate of diffusion and the net chemical production rate. In one dimension, this can be expressed as

$$\rho u \frac{d\alpha}{dx} = \text{diffusion rate} + \text{net chemical rate}$$

$$= \frac{d}{dx}\left(\rho D \frac{d\alpha}{dx}\right) + R_f - R_r \qquad (2)$$

where ρ, u, and D are the density, velocity, and diffusion coefficient, respectively, and R_f and R_r the forward and reverse chemical rate, respectively. Eleven chemical species (N_2, O_2, N, O, NO, N_2^+, O_2^+, N^+, O^+, NO^+, and e^-) must be accounted for in the AOTV flight regime and at least 20 chemical reactions occur significantly among these species in that regime. The reaction rate coefficients for these are known to within a factor of two to three (see, e.g., Ref. 22).

Behind a shock wave, a finite slope is produced in the concentration of all of these species. As a result, the species diffuse toward or away from the shock wave, depending on the sign of the slope. The rate and the extent of the diffusion depend on the slope in the concentration profile and gas density. In the low-density, high-speed flows produced by the AOTVs, the slopes are steep and the gas density is low,

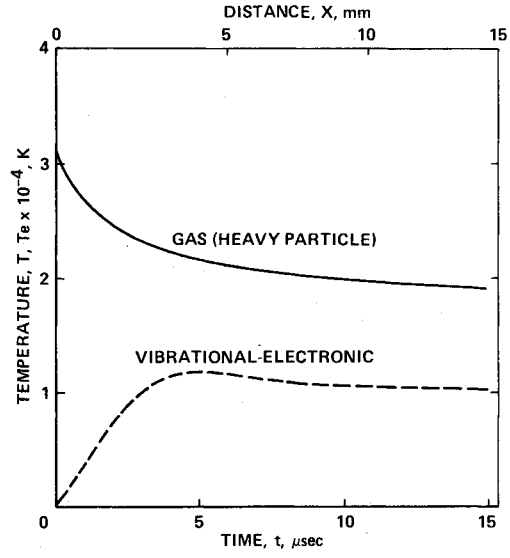

Fig. 12 Gas and vibrational-electron temperature calculated for an altitude of 80 km and a flight velocity of 9.6 km/s, neglecting transport phenomena.

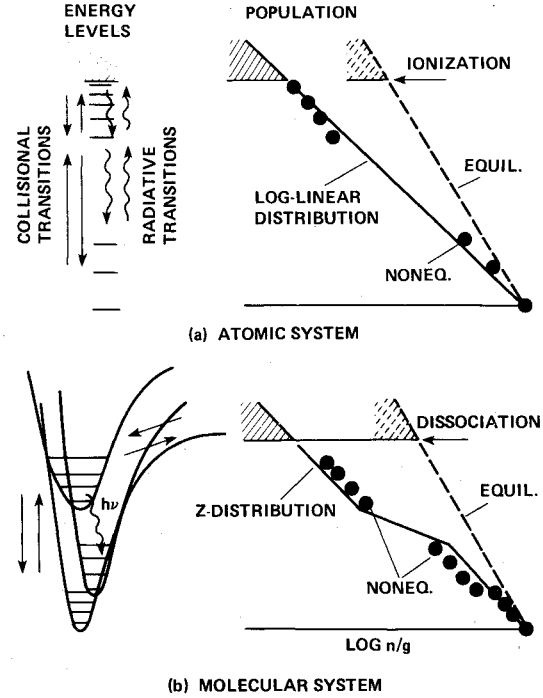

Fig. 13 Schematic of atomic and molecular systems under nonequilibrium excitation.

resulting in a strong diffusion. Since the shock wave does not create any of these species, the diffusion rate must be balanced by the convective transfer rate at the shock wave in the form

$$\rho u \alpha + \rho D \frac{d\alpha}{dx} = 0 \qquad (3)$$

This equation yields a finite value for the species concentration for all species at the shock wave. The value and the slope for the species concentration at the shock that is compatible with the condition that equilibrium be reached at $t = \infty$ must be found simultaneously with the solution of Eq. (2). The problem thus becomes elliptic; the numerical

procedure for solving the elliptic equation involving chemical rates has never been developed.

Of the four temperature modes mentioned above, rotational temperature tends to equilibrate very fast with the gas temperature and hence can be assumed to be equal to the gas temperature. The vibrational and electron temperatures tend to equal each other also because of a strong coupling between them.[20] Electron temperature dictates the collisional ionization rates and therefore must be determined accurately.[20] During a collisional ionization process, electron gas loses energy equal to the ionization potential. Conversely, the electron gas gains energy during a three-body electron recombination. Equilibration of the electron temperature with the gas temperature is slow because of the large disparity between the electron mass and heavy-particle mass. This causes a separation between the two temperatures.[21] The change in electron and vibrational temperature T_e can be calculated by accounting for all the energy inflows and outflows for the energy pool consisting of the electron gas energy and vibrational energy of the molecules. Denoting N_e and M as the number densities of electrons and molecules, respectively, and assuming that the energy loss by radiation is negligible, the rate of change of the combined energy pool is governed by

$$\rho u \frac{\mathrm{d}}{\mathrm{d}x}\left[\frac{(N_e+M)\,T_e}{\rho}\right] = \text{rate of heat conduction in electron gas} + \text{rate of energy gain by elastic collisions with heavy particles} + \text{rate of net energy gain during the inelastic (collisional ionization) processes} + \text{rate of energy gain due to collisional excitation of vibrational mode} \tag{4}$$

The expressions for the four terms in the right-hand side of Eq. (4) can be found from the literature.[16,21,23-26] The parameters characterizing the magnitudes of the first three terms in the right-hand side are known to within a factor of two to three. The vibrational relaxation rate coefficient appearing in the fourth term is known accurately[25] for temperatures below about 8000 K. Extrapolation of these values to the 30,000 K temperature that will be encountered in the AOTV flight regime leads to a logical inconsistency that the vibrational excitation cross section is diminishingly smaller than the elastic collision cross sections. Experience shows that the intensity of radiation from the nonequilibrium region behind a shock wave in the AOTV flight regime is severely affected (by several orders of magnitude) by the relaxation rate value in this high-temperature range.

The boundary conditions for Eq. (4) are determined by the phenomena ahead of the shock wave. Because of the heat conduction in the electron gas and absorption of radiation emitted by the gas behind the shock wave, the flow immediately ahead of the shock wave is probably ionized. Electron density and temperature become zero at the upstream edge of this ionized region. The boundary conditions at the shock wave are such that the values and the slopes of electron temperature and density must be continuous at the shock wave. These conditions must be compatible with those at $t=\infty$.

The global enthalpy of the gas H is a sum of all sensible modes of energy and the latent energies of all chemical species. Its rate of change is expressed, for the case in which energy loss by radiation is negligible, by

$$\rho u \frac{\mathrm{dH}}{\mathrm{d}x} = \frac{\mathrm{d}}{\mathrm{d}x}\left(k\frac{\mathrm{d}T}{\mathrm{d}x}\right) + \frac{\mathrm{d}}{\mathrm{d}x}\left[\rho D\left(1-\frac{1}{Le}\right)\sum h_i - \frac{\mathrm{d}\alpha_i}{\mathrm{d}x}\right] \tag{5}$$

where k is the thermal conductivity, Le the Lewis number, h_i the enthalpy of species i, and the summation is taken over all species i. If the Lewis number is assumed to be unity, this equation simplifies considerably. Otherwise, heat flow becomes significant and the problem with the boundary conditions arises.

To illustrate the extent of the separation between the heavy-particle and electron-vibrational temperature and the possibility of significant transport processes, a simple calculation is performed in the present study by neglecting the transport terms in these equations. All collisional reactions given in Ref. 22 are included for this calculation, with the rate coefficients given also in the reference. The vibrational relaxation time is expressed as the sum of the low- and high-temperature values. The low-temperature relaxation time is taken to be the nitrogen value given in Ref. 25. The high-temperature relaxation time is estimated using a hard-sphere collision model and choosing the excitation cross section so that the high-temperature relaxation time would be the same as the low-temperature relaxation time at the temperature of 10,000 K. This model reproduces the existing vibrational relaxation rate data for nitrogen at the low temperatures and yields a finite excitation cross section at high temperatures, although the absolute magnitude of the high-temperature value may not be correct. A typical result of this calculation is shown in Fig. 12. As seen here, there is a wide separation between the gas temperature and the vibrational-electron temperature in the altitude regime of interest. The slopes in the two temperature profiles are large behind the shock wave. From these, one sees the need to separately calculate the vibrational-electron temperature and the need to include the transport terms in the conservation equations.

Nonequilibrium Radiation

To calculate the intensity of radiation emitted by a gas under nonequilibrium conditions, one must first know the number densities of the upper and lower state of a particular optical transition. The ratio of the two number densities defines the so-called source function, or source temperature, in radiation transport, which is in general different from any of the four sensible temperatures mentioned earlier. The term excitation temperature is sometimes used to describe the source temperature.

The rate of change of the number density of any given internal state of an atom or a molecule n is a sum of the rate of diffusion and the net chemical production rate in exactly the same form as in Eq. (2). For the internal states, however, the chemical terms R_f and R_r are usually much larger than the diffusion term. To a first order, therefore, one can set

$$R_f - R_r = 0 \tag{6}$$

This is known as a quasi-steady-state condition. Equation (6) is written for all available internal states of atoms and molecules, resulting in a large system of algebraic equations.

In general, R_f and R_r consist of the sum of all collisional and radiative transitions. For radiative transitions, the rate of transition from the initial state i to the final state j, R_{ij} is expressed as

$$R_{ij} = A_{ij} n_i \text{ (radiative)} \tag{7}$$

where A_{ij} is the transition probability and n_i the number density of state i. For collisional transions, the rate becomes

$$R_{ij} = K_{ij} X n_i \text{ (collisional)} \tag{8}$$

where K_{ij} is the collisional transition rate coefficient and X the number density of the colliding particle causing the transition. The left sides of Figs. 13a and 13b schematically show the types of transitions involved. In both atomic and molecular systems, the transitions occur in four different

directions, that is, to and from the upper and lower states from the state under consideration. The destination of these transitions, suffixed j in Eqs. (7) and (8), must include all possible states in the system. The colliding partner X can be either a heavy particle or an electron. But electrons are several orders of magnitude more effective in causing the electronic and vibrational transitions than the heavy particles.[20] For these transitions, therefore, heavy-particle contributions can be neglected.

When all such transitions are summed up into Eq. (6), one obtains a system of simultaneous linear equations of an order equal to the number of available states, with the state densities n_i as the unknowns in the left-hand side and the concentrations of the gas species N_i as the known quantities in the right-hand side in the form,[23]

$$[B_{ij}]n_j = c_i N_i \tag{9}$$

The matrix $[B_{ij}]$ contains the collisional and radiative transition rate coefficients and the vector c_i specifies the equilibrium thermodynamic parameters. By solving Eq. (9), one obtains the distribution of number densities of all internal states. When the resulting n_i are divided by the multiplicity g_i and plotted in a semilogarithmic form, one obtains plots such as those shown in the right sides of Figs. 13a and 13b.

For atomic systems, the collisional and radiative transition rate coefficients are known to a fair accuracy. For the nitrogen atom, which is the most important atomic radiator in the AOTV flight regime, the excitation rate coefficients have been tabulated[24] and the state population distributions calculated using these excitation rates have been compared with experiment. Agreement between theory and experiment was good.[27] The right side of Fig. 13a shows typical such results. Shown also in the figure is a straight line connecting the ground state and the ionized state. The existing data indicate that, when the flow is ionized significantly, the population density distribution approximately follows this line. For a first approximation, therefore, this logarithmically linear distribution can be used for the AOTV calculation.

In the right side of Fig. 13b, the corresponding case of a molecular system is shown. Unlike the atomic systems, very little is known of the collisional transition rates in molecular systems. An effort was made in the present study to approximate the distribution by the one designated "Z distribution" in the figure, in which the upper state is assumed to be in equilibrium with the free (atomic) state while the lower state is in equilibrium with the ground state.[28] The resulting spectra were compared with the available experimental data. The calculated spectra did not resemble the observed spectra. It seems, therefore, that the distribution of the internal states of the molecular systems is more complex than in the case of atomic systems and cannot be modeled at present.

Approximate Computing Method

Because of the need to estimate the radiative heat fluxes to the AOTVs, an approximate calculation method was developed. This model assumes that the vibrational and electron temperatures are the same as the gas temperature; all transport phenomena are neglected. Ten chemical reactions are included in the calculation: $(O_2 + X \rightarrow O + O + X)$, $(N_2 + X \rightarrow N + N + X)$, $(NO + X \rightarrow N + O + X)$, $(NO + N \rightarrow O + N_2)$, $(NO + O \rightarrow O_2 + N)$, $(N + e \rightarrow N^+ + e + e)$, $(O + e \rightarrow O^+ + e + e)$, $(N_2^+ + e = N + N)$, $(NO^+ + e \rightarrow N + O)$, and $(O_2^+ + e \rightarrow O + O)$. The rate coefficients for these reactions are the same as those given in Ref. 22. The mechanisms of radiation included are 1) all atomic lines of N and O given in Ref. 29, 2) all atomic bound-free continuum of N and O given in Ref. 30, 3) N_2^+ first-negative band, 4) N_2 first-positive band, 5) N_2 second-positive band, 6) NO beta, 7) NO gamma, and 8) the O_2 Schumann-Runge band. The intensity parameters for the atomic lines are taken from Ref. 29, the continuum intensity parameters from Ref. 30, and the molecular bands from Ref. 31. Widths of the spectral lines are determined by the method given in Ref. 32 and the calculation is carried out line by line with the method described in Ref. 33.

In Fig. 7, the results of this calculation are compared with the experimental dta. The simple code produces results that agree fairly well with the laboratory data, especially at high flight velocities. At low velocities, the code overestimates by a factor of about three. As mentioned earlier, however, the experimental data at low velocities are likely to underestimate. Hence, the discrepancy between the present theoretical results and the experimental data is overlooked. In essence, the code is believed to be accurate to within a factor of about three. The code is used in Ref. 34 to compute the radiative heat fluxes for AOTVs.

Recommendations for Future Work

Both theoretical work and experimental work are needed in order to make reliable determinations of the raditive heat fluxes to the AOTVs. Experimentally, the scatter existing in the experimental data (see Fig. 6) must be narrowed. The factor-of-four scatter among the heat flux data shown in Fig. 7 is too large to be tolerated. The factor-of-three deviation between the present computed results and some of the experimental data points shown in Fig. 7 corresponds to an uncertainty in radiation-equilibrium wall temperature of a factor of 1.3, which is also intolerably large. The uncertainty concerning the transformation of the radiative heat flux data obtained at the side-on position (see Fig. 5) into the end-on position must be removed. Preferably, a radiation measurement would be made with a radiation sensor located at the stagnation point, as was done for the Apollo and Fire vehicles (see Fig. 5c). Both shock-tube and ballistic range facilities could be used for such a test. Whether and where the binary scaling law of nonequilibrium radiation is violated at the very low density owing to the collision-limiting phenomenon needs to be investigated. Experiments are needed also to provide physical property values for theoretical modeling. This includes: 1) vibrational relation rate coefficient at temperatures above 10,000 K; 2) excitation rate coefficients for molecules; and 3) spectral line widths, especially of molecules in an ionized regime. In addition, it would be desirable to improve the accuracy of the known chemical reaction rate coefficients and spectral intensity parameters.

Theoretical investigations must be made on several fronts also. Most urgent is the examination and analysis of the existing laboratory and flight data and their incorporation into a theoretical model. Theoretical calculation of physical properties such as vibrational relaxation rate, spectral intensity parameters, and line widths would be helpful in this endeavor. A numerical algorithm must be devised that accounts for the transport phenomena behind a shock wave and the precursor ionization. Coupling the chemical and kinetic models with a multidimensional flowfield calculation will be a hard task also. The chemical and kinetic equations describing the physicochemical phenomena are large in number and are very stiff and therefore would consume an unacceptably large computing time. The flowfield calculation must be of the full viscous shock-layer type with finite rate chemistry. The boundary conditions at the wall for the various properties involved must be examined also.

Conclusions

Existing experimental data obtained in shock tubes and ballistic ranges indicate that the radiation from a shock layer in the nonequilibrium regime expected of the aeroassisted orbital transfer vehicles is of the same order as the convective heat-transfer rates to the vehicles, but the rates are uncertain to within a factor of three. Measurements with the Fire vehicles yielded small values of the radiation rates because of

the truncation phenomenon, and the Apollo experiment resulted in small values because of the combination of boundary-layer blowing and truncation. Many problems exist in modeling the nonequilibrium radiation theoretically, but an approximate computing method that roughly reproduces the existing experimental data has been introduced. Further experimental work and theoretical work are needed in order to improve the reliability of the radiative heat-transfer rate predictions.

References

[1] "Orbital Transfer Vehicle Concept Definition Study," The Boeing Company, Rept. D180-26090, Vols. 1-6, 1980.

[2] "Orbital Transfer Vehicles (OTV) Concept Definition Study," General Dynamics-Convair Div., Rept. GDC-ASP-80-012, Vols. 1-6, 1981.

[3] London, H.S., "Changes of Satellite Orbit by Aerodynamic Maneuvering," *Journal of the Aerospace Sciences,* Vol. 29, March 1962, pp. 323-332.

[4] Hornby, H. and Allen, W.H., "Mission to the Libration Centers," *Astronautics and Aeronautics,* Vol. 4, July 1966, pp. 78-82.

[5] Candra, E. and Arthur, P.D., "Orbit Plane Change by External Burning Aerocruise," *Journal of Spacecraft and Rockets,* Vol. 3, March 1966, pp. 347-352.

[6] Camm, J.C., Kivel, B., Taylor, R.L., and Teare, J.D., "Absolute Intensity of Nonequilibrium Radiation in Air and Stagnation Heating at High Altitudes," AVCO-Everett Res. Lab., Everett, Mass., Res. Rept. 93, 1959.

[7] Teare, J.D., Georgiev, S., and Allen, R.A., "Radiation From the Nonequilibrium Shock Front," AVCO-Everett Res. Lab., Everett, Mass., Res. Rept. 112, 1961.

[8] Allen, R.A., Rose, P.H., and Camm, J.C., "Nonequilibrium and Equilibrium Radiation at Super-Satellite Reentry Velocities," AVCO-Everett Res. Lab., Everett, Mass., Res. Rept. 156, 1962.

[9] Canning, T.N. and Page, W.A., "Measurement of Radiation from the Flow Fields of Bodies Flying at Speeds up to 13.4 Kilometers per Second," Paper presented as AGARD Fluid Mechanics Panel, Brussels, April 1962.

[10] Page, W.A. and Arnold, J.O., "Shock Layer Radiation of Blunt Bodies at Entry Velocities," NASA TR R-193, 1964.

[11] Cauchon, D.L., "Project Fire Flight 1 Radiative Heating Experiment," NASA TM X-1222, 1966.

[12] Cauchon, D.L., "Radiative Heating Results from the Fire 2 Flight Experiment at a Reentry Velocity of 11.4 Kilometers per Second," NASA TM X-1402, 1967.

[13] Lee, D.B. and Goodrich, W.D., "The Aerothermodynamic Environment of the Apollo Command Module during Super-orbital Entry," NASA TN D-6792, 1972.

[14] Curry, D.M. and Stephens, E.W., "Apollo Ablator Thermal Performance at Super-Orbital Entry Velocities," NASA TN D-5969, 1970.

[15] Hansen, C.F., "Approximations for the Thermodynamic and Transport Properties of High-Temperature Air," NASA TR R-50, 1959.

[16] Okuno, A.F. and Park, C., "Stagnation-Point Heat Transfer Rate in Nitrogen Plasma Flows: Theory and Experiment," *Transactions of ASME,* Ser. C., *Journal of Heat Transfer,* Vol. 92, No. 3, Aug. 1970, pp. 372-384.

[17] Bartlett, E.P. and Anderson, L.W., "An Evaluation of Ablation Mechanisms for the Apollo Heat Shield Material," AIAA Paper 69-98, Jan. 1969.

[18] Kottock, S., "The Development of a Phenolic Nylon Model for a Reaction Kinetics Ablation Program," Missile and Space Div., General Electric Co., Valley Forge, Pa., Tech. Info. Series No. 65SD320, 1965.

[19] Fay, J.A. and Riddell, F.R., "Theory of Stagnation Point Heat Transfer in Dissociated Air," *Journal of the Areonautical Sciences,* Vol. 25, Feb. 1958, pp. 73-97.

[20] Massey, H.S.W. and Burhop, E.H.S., *Electronic and Ionic Impact Phenomena,* Oxford University Press, London, 1954.

[21] Appleton, J.P. and Bray, K.N.C., "The Conservation Equation for a Nonequilibrium Plasma," *Journal of Fluid Mechanics,* Vol. 20, No. 4, Dec. 1964, pp. 659-672.

[22] Park, C. and Menees, G.P., "Odd Nitrogen Production by Meteoroids," *Journal of Geophysical Research,* Vol. 83, Aug. 1978, pp. 4029-4035.

[23] Bowen, S.W. and Park, C., "Computer Study of Nonequilibrium Excitation in Recombining Nitrogen Plasma Nozzle Flows," *AIAA Journal,* Vol. 9, March 1971, pp. 493-499.

[24] Park, C., "Comparison of Electron and Electronic Temperatures in Recombining Nozzle Flow of Ionized Nitrogen-Hydrogen Mixture, Part 1, Theory," *Journal of Plasma Physics,* Vol. 9, Pt. 2, July 1973, pp. 187-215.

[25] Millikan, R.C. and White, D.R., "System of Vibrational Relaxation," *Journal of Chemical Physics,* Vol. 39, Dec. 1963, pp. 3209-3213.

[26] Yos, J.M., "Transport Properties of Nitrogen, Hydrogen, Oxygen, and Air to 30,000 K," AVCO-RAD, Wilmington, Mass., Tech. Memo. RAD TM-63-7, 1963.

[27] Park, C., "Comparison of Electron and Electronic Temperatures in Recombining Nozzle Flow of Ionized Nitrogen-Hydrogen Mixture, Part 2, Experiment," *Journal of Plasma Physics,* Vol. 9, Pt. 2, July 1973, pp. 217-234.

[28] Flagan, R.C. and Appleton, J.P., "Excitation Mechanism of the Nitrogen First-Positive and First-Negative Radiation at High Temperature," *Journal of Chemical Physics,* Vol. 56, No. 3, Feb. 1972, pp. 1163-1173.

[29] Wiese, W.L., Smith, M.W., and Glennon, B.M., *Atomic Transition Probabilities, Vol. 1: Hydrogen through Neon,* National Standard Reference Data Series-National Bureau of Standards, NSRDS-NBS 4, May 1966.

[30] Peach, G., "Continuous Absorption Coefficients for Non-Hydrogenic Atoms," *Memoirs of the Royal Astronomical Society,* Vol. 73, 1970, pp. 1-123.

[31] Allen, R.A., "Air Radiation Tables: Spectral Distribution Functions for Molecular Band Systems," AVCO-Everett Res. Lab., Everett, Mass., Res. Rept. 236, 1966.

[32] Park, C., "Radiation Enhancement by Nonequilibrium during Flight through the Titan Atmosphere," AIAA Paper 82-0878, June 1982.

[33] Arnold, J.O., Cooper, D.M., Park, C., and Prakash, S.G., "Line-by-line Transport Calculations for Jupiter Entry Probes," *Progress in Astronautics and Aeronautics: Entry Heating and Thermal Protection,* Vol. 69, edited by W.G. Olstad, American Institute of Aeronautics and Astronautics, New York, 1980, pp. 52-82.

[34] Menees, G.P., "Trajectory Analysis of Radiative Heating for Planetary Missions with Aerobraking of Spacecraft," *Journal of Spacecraft and Rockets,* Vol. 22, Jan.-Feb. 1985, pp. 37-45.